Reactions of Group V Metal Atoms with Water Molecules. Matrix Isolation FTIR and Quantum Chemical Studies

Mingfei Zhou,* Jian Dong, Luning Zhang, and Qizong Qin

Contribution from the Department of Chemistry, Laser Chemistry Institute, Fudan University, Shanghai, P. R. China

Received August 17, 2000

Abstract: Laser-ablated group V metal atoms (V, Nb, Ta) were co-deposited with water molecules in excess argon. The V atoms reacted with water to form the inserted HVOH molecule spontaneously. The Nb atoms reacted with water to form the $NbOH_2$ complex and the inserted HNbOH molecule. Broad-band photolysis produced the H_2VO and H_2NbO molecules as well as the VO and NbO monoxides. For Ta + H_2O reactions, neither $TaOH_2$ nor HTaOH was observed, while the H_2TaO molecule was produced on annealing, and the H_2 elimination process was not observed on photolysis. The aforementioned species were identified via isotopic substitutions as well as density functional calculations. Qualitative analysis of the possible reaction paths leading to the observed products is proposed. The results have been compared with our earlier works concerning the Sc and group IV metal atoms with water reactions in order to observe existent trends for the early transition metal atoms.

Introduction

The interaction of transition metal atoms and cations with water molecules has attracted considerable attentions. The $M^+ + H_2O \rightarrow MO^+ + H_2$ and its reverse reactions in the gas phase have been studied both experimentally and theoretically.[1−14] It was found that early transition metal cations (Sc^+, Ti^+, V^+) are more reactive than their oxides, and the formation of the low-lying states $MO^+ + H_2$ is the only exothermic process.[1−3,12,13] But for middle transition metals, the oxides are more reactive than the metal cations. However, the reactions of transition metal atoms and water molecules have received far less attention. Lin and Parson reported that atomic Sc reacted with water to give ScO in the gas phase.[15] Matrix isolation infrared absorption studies reported by Kauffman et al. showed that thermal Sc, Ti, and V atoms could react with water to form the insertion products spontaneously, while the late transition metal atoms reacted with water to form metal−water adducts. These adducts rearranged to the insertion molecules on photolysis.[16,17]

Recently, we performed matrix isolation FTIR and theoretical study of reactions of laser-ablated Sc and group IV metal atoms with water molecules in solid argon.[18,19] For Sc, the difference between laser ablated and thermal evaporated Sc atom reactions is the observation of HScO and ScOH molecules with laser ablation. Of more importance, a new reaction path leading to the formation of H_2MO (M = Ti, Zr, Hf) was observed for group IV metal atoms. Here we report the reactions of group V metal atoms with water molecules, completing our study on the early transition metal atoms and water molecule reactions.

Experimental and Theoretical Methods

The experimental setup for pulsed laser ablation and matrix infrared spectroscopic investigation has been described previously[20] and is similar to the technique employed earlier by the Andrews group.[21] The 1064-nm Nd:YAG laser fundamental (Spectra Physics, DCR 150, 20-Hz repetition rate and 8-ns pulse width) was focused onto the rotating metal target through a hole in a CsI window, and the ablated metal atoms were co-deposited with H_2O in excess argon onto an 11 K CsI window, which was mounted on a cold tip of a closed-cycle helium refrigerator (Air Products, model CSW202) for 1 h at a rate of 2−4 mmol/h. Typically, 5−10 mJ/pulse laser power was used. H_2O, $H_2{}^{18}O$ (96%^{18}O) and D_2O were subjected to several freeze−pump−thaw cycles before use. Infrared spectra were recorded on a Bruker IFS113V

* Corresponding author: (e-mail) mfzhou@srcap.stc.sh.cn; (fax) 0086-21-65102777.

(1) Clemmer, D. E.; Aristov, N.; Armentrout, P. B. *J. Phys. Chem.* **1993**, *97*, 544.
(2) Chen, Y. M.; Clemmer, D. E.; Armentrout, P. B. *J. Phys. Chem.* **1994**, *98*, 11490.
(3) Guo, B. C.; Kerns, K. P.; Castleman, A. W. *J. Phys. Chem.* **1992**, *96*, 4879.
(4) Ryan, M. F.; Fiedler, A.; Schroder, D.; Schwarz, H. *J. Am. Chem. Soc.* **1995**, *117*, 2033.
(5) Schroder, D.; Fiedler, A.; Ryan, M. F.; Schwarz, H. *J. Phys. Chem.* **1994**, *98*, 68.
(6) Clemmer, D. E.; Chen, Y. M.; Khan, F. A.; Armentrout, P. B. *J. Phys. Chem.* **1994**, *98*, 6522.
(7) Tilson, J. L.; Harrison, J. F. *J. Phys. Chem.* **1991**, *95*, 5097.
(8) Fiedler, A.; Schroder, D.; Shaik, S.; Schwarz, H. *J. Am. Chem. Soc.* **1994**, *116*, 10734.
(9) Danovich, D.; Shaik, S. *J. Am. Chem. Soc.* **1997**, *119*, 1773.
(10) Ye, S. *Theochem* **1997**, *417*, 157.
(11) Irigoras, A.; Fowler, J. E.; Ugalde, J. M. *J. Phys. Chem. A* **1998**, *102*, 293.
(12) Irigoras, A.; Fowler, J. E.; Ugalde, J. M. *J. Am. Chem. Soc.* **1999**, *121*, 574.
(13) Irigoras, A.; Fowler, J. E.; Ugalde, J. M. *J. Am. Chem. Soc.* **1999**, *121*, 8549.
(14) Irigoras, A.; Fowler, J. E.; Ugalde, J. M. *J. Am. Chem. Soc.* **2000**, *122*, 114.
(15) Liu, K.; Parson, J. M. *J. Chem. Phys.* **1978**, *68*, 1794.
(16) Kauffman, J. W.; Hauge, R. H.; Margrave, J. L. *J. Phys. Chem.* **1985**, *89*, 3541.
(17) Kauffman, J. W.; Hauge, R. H.; Margrave, J. L. *J. Phys. Chem.* **1985**, *89*, 3547.
(18) Zhang, L.N.; Dong, J.; Zhou, M. F. *J. Phys. Chem. A*, **2000**, *104*, 8882.
(19) Zhou, M. F.; Zhang, L. N.; Dong, J.; Qin, Q. Z. *J. Am. Chem. Soc.* **2000**, *122*, 10680.
(20) Chen, M. H.; Wang, X. F.; Zhang, L. N.; Yu, M.; Qin, Q. Z. *Chem. Phys.* **1999**, *242*, 81.
(21) Burkholder, T. R.; Andrews, L. *J. Chem. Phys.* **1991**, *95*, 8697.

10.1021/ja003072z CCC: $20.00
Published on Web 12/14/2000

spectrometer at 0.5-cm^{-1} resolution using a DTGS detector. Matrix samples were annealed at different temperatures, and selected samples were subjected to broad-band photolysis using a high-pressure mercury lamp.

Quantum chemical calculations were performed using the Gaussian 98 program.[22] The three-parameter hybrid functional according to Becke with additional correlation corrections due to Lee, Yang, and Parr were utilized (B3LYP).[23,24] Recent calculations have shown that this hybrid functional can provide accurate results for the geometries and vibrational frequencies for transition metal-containing compounds.[12−14,25−29] The 6-311++G(d,p) basis sets were used for H and O atoms, the all electron basis sets of Wachters−Hay as modified by Gaussian were used for V atom, and the Los Alamos ECP plus DZ were used for Nb and Ta atoms.[30−32] These ECPs incorporate the mass velocity and Darwin relativistic effects into the potential. Reactants, various possible transition states, intermediates, and products were optimized. The vibrational frequencies were calculated with analytic second derivatives, and zero point vibrational energies (ZPVE) were derived.

Results and Discussion

Infrared Spectra. Experiments were done with water concentrations ranging from 0.2 to 0.5% in argon, and typical infrared spectra for the reactions of laser-ablated V, Nb, and Ta atoms with water molecules in excess argon in the selected regions are shown in Figures 1−3, respectively, and the product absorptions are listed in Table 1. The stepwise annealing and photolysis behavior of the product absorptions is also shown in the figures and will be discussed below. Experiments were also done with D_2O and $H_2{}^{18}O$ samples, and the representative spectra in selected regions are shown in Figures 4−6, respectively.

Calculation Results. Calculations were done on three isomers of MH_2O, namely, the inserted HMOH molecules, the H_2MO molecules, and the MOH_2 complexes. The geometric parameters and relative stabilities are shown in Figure 7, and the vibrational frequencies and intensities are listed in Tables 2−4. For the inserted HMOH molecules, stable minimums have been found on both the quartet and doublet potential energy surfaces, but no stable structure was found on the sextet potential energy surface. All three inserted HMOH molecules were calculated to have $^4A''$ ground states. For MOH_2, only the states that correlated to the ground-state metal atoms were calculated.[33] The VOH_2 has a $^4B_1$ ground state with planar C_{2v} symmetry.

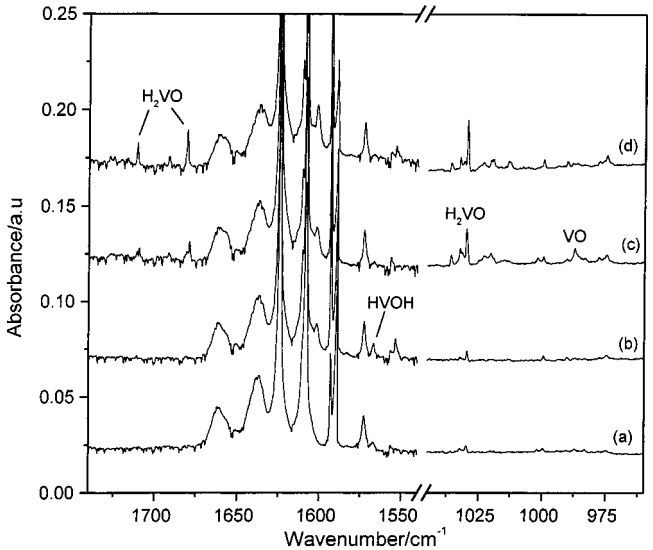

Figure 1. Infrared spectra in the 1740−1540- and 1040−960-cm^{-1} regions from co-deposition of laser-ablated V with 0.2% water in argon: (a) 1-h sample deposition at 11 K, (b) 25 K annealing, (c) 20-min broad-band photolysis, and (d) annealing to 30 K.

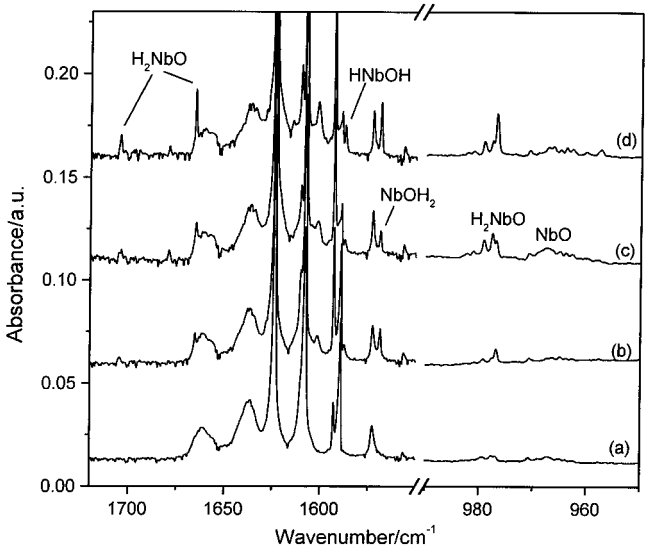

Figure 2. Infrared spectra in the 1720−1550- and 990−950-cm^{-1} regions from co-deposition of laser-ablated Nb with 0.2% water in argon: (a) 1-h sample deposition at 11 K, (b) 25 K annealing, (c) 20-min broad-band photolysis, and (d) annealing to 30 K.

The $NbOH_2$ and $TaOH_2$ were predicted to have $^6A'$ and $^4A''$ ground states with nonplanar geometry. All three H_2MO molecules were predicted to have $^2A'$ ground states with nonplanar geometry. At the B3LYP level of theory, the $^4A''$ HVOH was predicted to be the most stable structure followed by the $^2A'$ H_2VO molecule. For Nb and Ta, the $^2A'$ H_2MO molecules are more stable than the inserted HMOH molecules and the MOH_2 complexes.

B3LYP calculations were also done on monoxides, and the results are listed in Table 5. Both VO and NbO were predicted to have $^4\Sigma^-$ ground states, while TaO was calculated to have a $^2\Delta$ ground state, in agreement with previous reports.[34−38]

(22) Gaussian 98, Revision A.7. Frisch, M. J.; Trucks, G. W.; Schlegel, H. B.; Scuseria, G. E.; Robb, M. A.; Cheeseman, J. R.; Zakrzewski, V. G.; Montgomery, J. A., Jr.; Stratmann, R. E.; Burant, J. C.; Dapprich, S.; Millam, J. M.; Daniels, A. D.; Kudin, K. N.; Strain, M. C.; Farkas, O.; Tomasi, J.; Barone, V.; Cossi, M.; Cammi, R.; Mennucci, B.; Pomelli, C.; Adamo, C.; Clifford, S.; Ochterski, J.; Petersson, G. A.; Ayala, P. Y.; Cui, Q.; Morokuma, K.; Malick, D. K.; Rabuck, A. D.; Raghavachari, K.; Foresman, J. B.; Cioslowski, J.; Ortiz, J. V.; Baboul, A. G.; Stefanov, B. B.; Liu, G.; Liashenko, A.; Piskorz, P.; Komaromi, I.; Gomperts, R.; Martin, R. L.; Fox, D. J.; Keith, T.; Al-Laham, M. A.; Peng, C. Y.; Nanayakkara, A.; Gonzalez, C.; Challacombe, M.; Gill, P. M. W.; Johnson, B.; Chen, W.; Wong, M. W.; Andres, J. L.; Gonzalez, C.; Head-Gordon, M.; Replogle, E. S.; Pople, J. A. Gaussian, Inc.: Pittsburgh, PA, 1998.

(23) Becke, A. D. *J. Chem. Phys.* **1993**, *98*, 5648.

(24) Lee, C.; Yang, E.; Parr, R. G. *Phys. Rev. B* **1988**, *37*, 785.

(25) Bauschlicher, C. W., Jr.; Ricca, A.; Partridge, H.; Langhoff, S. R. In *Recent Advances in Density Functional Theory*; Chong, D. P., Ed.; World Scientific Publishing: Singapore, 1997; Part II.

(26) Bytheway, I.; Wong, M. W. *Chem. Phys. Lett.* **1998**, *282*, 219.

(27) Siegbahn, P. E. M. *Electronic Structure Calculations for Molecules Containing Transition Metals. Adv. Chem. Phys.* **1996**, XCIII.

(28) Bauschlicher, C.W., Jr.; Maitre, P. *J. Chem. Phys.* **1995**, *99*, 3444.

(29) Hartmann, M.; Clark, T.; Van Eldik, R. *J. Am. Chem. Soc.* **1997**, *119*, 7843.

(30) McLean, A. D.; Chandler, G. S. *J. Chem. Phys.* **1980**, *72*, 5639. Krishnan, R.; Binkley, J. S.; Seeger, R.; Pople, J. A. *J. Chem. Phys.* **1980**, *72*, 650.

(31) Wachter, J. H. *J. Chem. Phys.* **1970**, *52*, 1033. Hay, P. J. *J. Chem. Phys.* **1977**, *66*, 4377.

(32) Hay, P. J.; Wadt, W. R. *J. Chem. Phys.* **1985**, *82*, 299.

(33) Moore, C. E. *Atomic Energy Levels*; National Bureau of Standards: Washington, DC, 1959.

(34) Weltner, W., Jr.; McLeod, D., Jr. *J. Chem. Phys.* **1965**, *42*, 882.

(35) Brom, J. M.; Durham, C. H.; Weltner, W., Jr. *J. Chem. Phys.* **1974**, *61*, 970.

(36) Dyke, J. M.; Ellis, A. M.; Feher, M.; Morris, A.; Paul, A. J.; Stevens, J. C. H. *J. Chem. Soc. Faraday Trans.* **1987**, *83*, 1555.

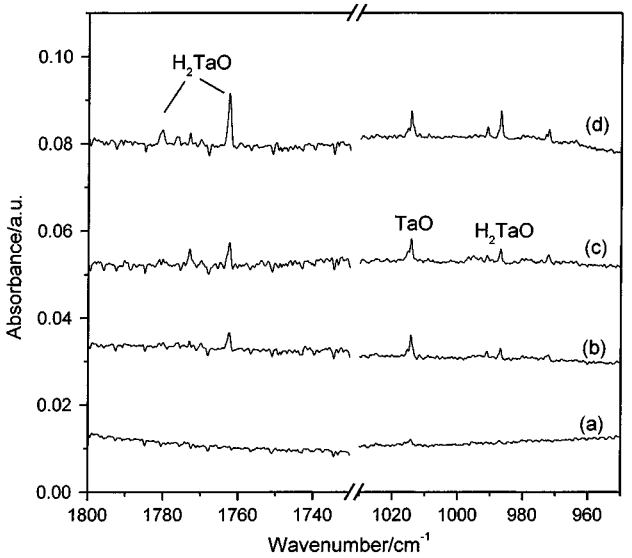

Figure 3. Infrared spectra in the 1800−1730- and 1030−950-cm^{-1} regions from co-deposition of laser-ablated Ta with 0.2% water in argon: (a) 1-h sample deposition at 11 K, (b) 25 K annealing, (c) 20-min broad-band photolysis, and (d) annealing to 30 K.

Table 1. Infrared Absorptions (cm^{-1}) from Co-Deposition of Laser-Ablated V, Nb, and Ta Atoms with Water Molecules in Excess Argon

H_2O	D_2O	$H_2{}^{18}O$	assignment
		(a) V + H_2O/Ar	
1710.6	1235.1	1710.6	H_2VO sym−VH_2
1680.4	1215.3	1680.4	H_2VO asy−VH_2
1567.0	1128.4	1567.0	HVOH V−H
1035.9	1035.5	992.0	H_2VO site
1032.3	1031.9	988.2	H_2VO site
1029.4	1029.1	986.4	H_2VO V−O
987.3	987.3	944.9	VO
		(b) Nb + H_2O/Ar	
1704.5	1224.0	1704.5	H_2NbO sym−NbH_2
1665.2	1197.7	1665.2	H_2NbO asy−NbH_2
1587.5	1141.2		HNbOH Nb−H
1569.1	1153.2	1567.0	$NbOH_2$ H_2O bending
979.2	978.4	932.6	H_2NbO site
976.9	976.1	930.4	H_2NbO Nb−O
970.7	970.7	923.7	NbO
966.5	966.5	920.4	NbO site
		(c) Ta + H_2O/Ar	
1780.4		1780.8	H_2TaO sym−TaH_2
1762.3	1264.7	1762.7	H_2TaO asy−TaH_2
1014.4	1014.4	961.4	TaO
986.9	984.9	936.7	H_2TaO Ta−O

MO. The 987.3-cm^{-1} band was produced only on broad-band photolysis; it exhibited no deuterium isotopic shift but was shifted to 944.9 cm^{-1} with $H_2{}^{18}O$, and gave an isotopic 16/18 ratio of 1.0449. This band is assigned to the VO molecule, which is in good agreement with recent matrix isolation study of V + O_2 reaction.[37] The vibrational fundamental of VO was predicted at 1040 cm^{-1} at the B3LYP/6-311+G(d) level.

In the Nb + H_2O experiments, a broad band centered at 966.5 cm^{-1} was also produced on broad-band photolysis. It showed the diatomic Nb−O stretching vibrational frequency ratio, and only one oxygen atom is involved. This band was also observed on (Nb + O_2)/Ar experiments[38] and is assigned to the NbO molecule. The NbO was predicted to have $^4\Sigma^-$ ground state with vibrational fundamental at 976 cm^{-1}.

(37) Chertihin, G. V.; Bare, W. D.; Andrews, L. *J. Phys. Chem. A* **1997**, *101*, 5090.

(38) Zhou, M. F.; Andrews, L. *J. Phys. Chem. A* **1998**, *102*, 8251.

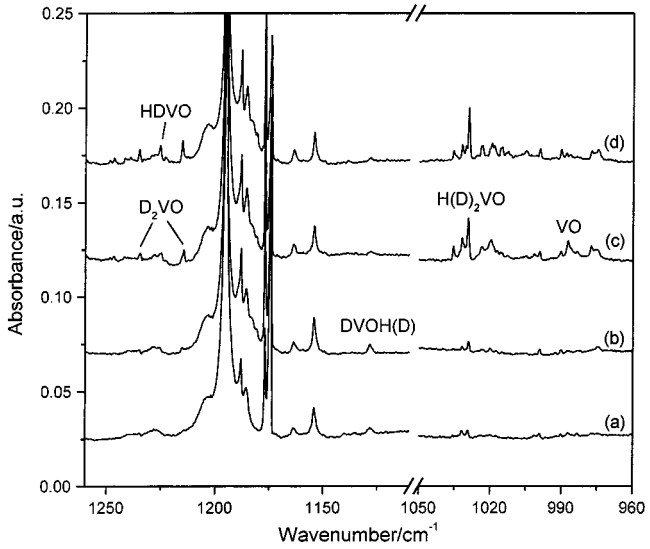

Figure 4. Infrared spectra in the 1260−1120- and 1050−960-cm^{-1} regions from co-deposition of laser-ablated V with 0.4% (H_2O + HDO + D_2O) in argon: (a) 1-h sample deposition at 11 K, (b) 25 K annealing, (c) 20-min broad-band photolysis, and (d) annealing to 30 K.

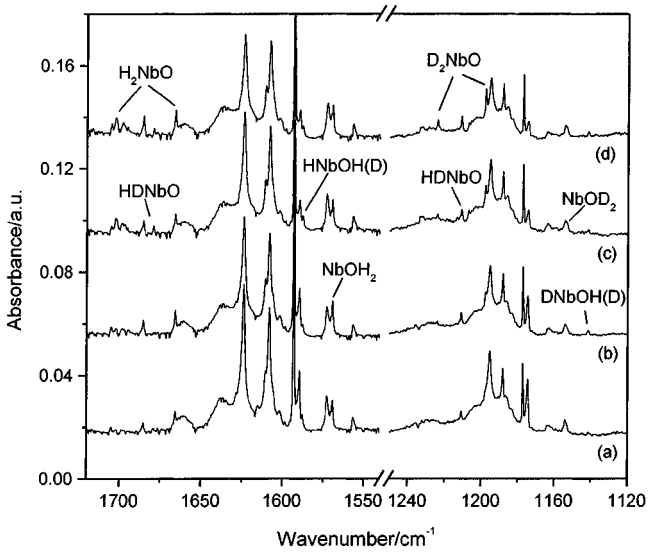

Figure 5. Infrared spectra in the 1720−1540- and 1250−1120-cm^{-1} regions from co-deposition of laser-ablated Nb with 0.4% (H_2O + HDO + D_2O) in argon: (a) 1-h sample deposition at 11 K, (b) 25 K annealing, (c) 20-min broad-band photolysis, and (d) annealing to 30 K.

The 1014.4-cm^{-1} band in the Ta + H_2O experiments is assigned to the TaO molecule based on isotopic substitution experiments and previous work.[34,38] This molecule was predicted to have a $^2\Delta$ ground state with vibrational fundamental at 1028 cm^{-1}.

No MO_2 (M = V, Nb, Ta) absorptions was observed in these experiments.[37,38]

MOH_2. The 1569.1-cm^{-1} band in the Nb + H_2O experiments markedly increased on annealing but decreased on broad-band photolysis. It shifted to 1153.2 cm^{-1} with D_2O and to 1567.0 cm^{-1} with $H_2{}^{18}O$. The isotopic H/D ratio of 1.3606 and $^{16}O/^{18}O$ ratio of 1.0013 indicate a H_2O bending vibration. The isotopic doublet structure observed in the mixed $H_2{}^{16}O$ + $H_2{}^{18}O$ experiment confirms that only one H_2O unit is involved. The 1569.1-cm^{-1} band is assigned to the H_2O bending vibration of the $NbOH_2$ complex. DFT calculation predicted that $NbOH_2$ has a $^6A'$ ground state, with a H_2O bending vibration at 1603 cm^{-1}, and isotopic frequency ratios in good agreement with

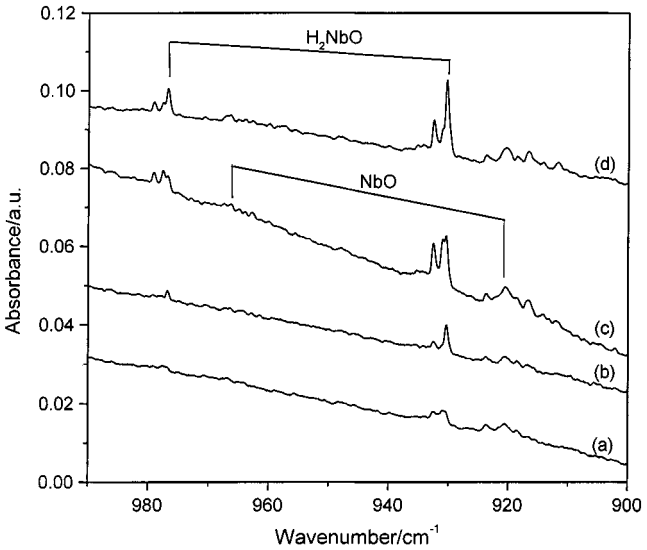

Figure 6. Infrared spectra in the 990−900-cm^{-1} region from co-deposition of laser-ablated Nb with 0.4% ($H_2{}^{16}O + H_2{}^{18}O$) in argon: (a) 1-h sample deposition at 11 K, (b) 25 K annealing, (c) 20-min broad-band photolysis, and (d) annealing to 30 K.

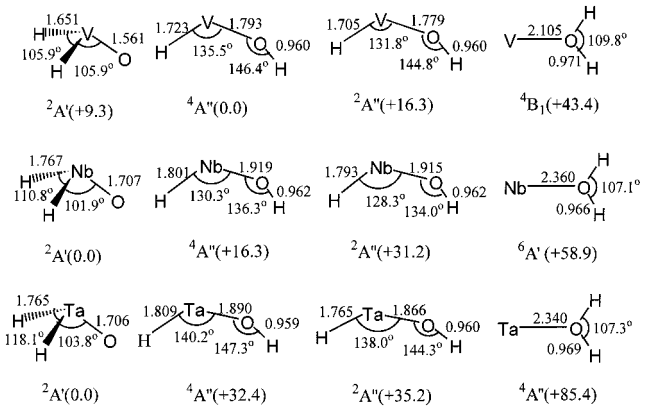

Figure 7. B3LYP calculated geometric parameters (bond length in Å, bond angle in degree) and relative stability (kcal/mol) of the MH_2O (M = V, Nb, Ta) isomers.

Table 2. Calculated Vibrational Frequencies (cm^{-1}) and Intensities (km/mol) for HVOH, H_2VO, VOH_2, and the Transition States (TS1, TS2) on the V + H_2O Reaction Paths

HVOH(^{4}A″)	HVOH (^{2}A″)	H_2VO(^{2}A′)	VOH_2($^4B_1$)	TS1	TS2
3901(136)	3888(140)	1815(138)	3737(12)	1769	1878
1635(334)	1663(332)	1778(337)	3624(517)	1707	1736
714(181)	732(182)	1113(217)	1564(133)	987	1093
518(135)	542(108)	628(79)	390(4)	539	895
447(289)	453(264)	534(10)	318(5)	471	838
287(189)	317(167)	506(171)	132(89)	1766i	1295i

experimental values (calculated isotopic ratios: H/D 1.3641, $^{16}O/^{18}O$ 1.0043).

No evidence was found for the VOH_2 and $TaOH_2$ complexes. DFT calculations predicted that VOH_2 has a $^4B_1$ ground state with a H_2O bending vibration at 1564 cm^{-1}. The $TaOH_2$ has a ^{4}A″ ground state with a H_2O bending vibration at 1595 cm^{-1}.

HMOH. The 1567.0-cm^{-1} band in the V + H_2O experiments increased on 25 K annealing but was destroyed on broad-band photolysis, while annealing to 30 K allowed regeneration of this band. This band showed a negligible oxygen-18 shift, but was shifted to 1128.0 cm^{-1} with D_2O and gave an isotopic H/D ratio of 1.3892. The isotopic shifts suggest assignment to a V−H stretching mode. Photolysis destroyed the 1567.0-cm^{-1} band with the H_2VO absorptions greatly enhanced, suggesting that the 1567.0-cm^{-1} band may due to a vibrational mode of a structural isomer of the H_2VO molecule. This band is assigned to the V−H stretching vibration of the HVOH molecule following the HScOH and HTiOH examples.[18,19] Present DFT calculations predicted the HVOH to have a ^{4}A″ ground state with bent geometry and is the most stable structural isomer of V−H_2O. The V−H and V−OH stretching vibrational modes were calculated at 1635 and 714 cm^{-1} with 334:177 relative intensities. Our spectrum below the 700-cm^{-1} region is noisy, and the V−OH mode was not observed. In previous thermal V atom and water reaction study, absorptions at 1583.0 and 703.3 cm^{-1} were assigned to the V−H and V−OH stretching modes of the HVOH molecule.[17] No absorption around 1583 cm^{-1} was observed in our experiments. We note that previous thermal experiments were performed at 15 K and employed higher metal and water concentrations than our laser ablation experiments. We suggest that the 1583.0- and 703.3-cm^{-1} absorptions in previous experiments were most probably due to cluster species.

Table 3. Calculated Vibrational Frequencies (cm^{-1}) and Intensities (km/mol) for HNbOH, H_2NbO, $NbOH_2$ and the Transition States (TS1, TS2) on the Nb + H_2O Reaction Paths

HNbOH(^{4}A″)	HNbOH(^{2}A″)	H_2NbO(^{2}A′)	$NbOH_2$(^{6}A′)	TS1	TS2
3864(153)	3858(161)	1785(142)	3839(72)	1785	1859
1671(342)	1686(324)	1758(385)	3737(29)	1664	1738
691(139)	696(134)	1000(179)	1603(104)	910	978
577(77)	579(74)	625(113)	432(3)	521	924
494(208)	441(210)	571(16)	304(249)	438	809
345(176)	354(162)	535(141)	274(8)	1542i	1368i

The weak band at 1587.5 cm^{-1} in the Nb + H_2O experiments is assigned to the Nb−H stretching vibration of the HNbOH molecule. The deuterium counterpart is observed at 1141.2 cm^{-1}, which gave an isotopic H/D ratio of 1.3911. DFT calculations predicted that the HNbOH molecule has a ^{4}A″ ground state, which is ∼16.3 kcal/mol higher in energy than the ^{2}A′ H_2NbO molecule. The strongest absorption of the HNbOH molecule is the Nb−H stretching vibration calculated at 1671 cm^{-1}.

H_2MO. In the V + H_2O reaction, absorptions at 1029.4, 1680.4, and 1710.6 cm^{-1} can be grouped together by their consistent behavior upon annealing and photolysis. These bands were weaker on sample deposition, but were greatly enhanced on broad-band photolysis, and sharpened on 30 K annealing. The 1029.4-cm^{-1} band shifted to 986.4 cm^{-1} with $H_2{}^{18}O$ sample and gave a $^{16}O/^{18}O$ isotopic ratio of 1.0436, suggesting that this band is mainly due to a terminal V−O stretching vibration. This band has been assigned to the VO molecule in previous thermal V atom reactions with water in solid argon.[17] However, this band was not observed in the V + O_2 reactions in solid argon.[33] Of more importance, it shifted to 1029.1 cm^{-1} with D_2O sample; the 0.3-cm^{-1} deuterium isotopic shift indicates that this band is not due to a pure V−O stretching vibration and is slightly perturbed by hydrogen atoms. In concert, the 1680.4- and 1710.6-cm^{-1} bands showed no oxygen-18 shift with $H_2{}^{18}O$ sample but were shifted to 1215.3 and 1235.1 cm^{-1} with D_2O sample and gave isotopic H/D ratios of 1.3827 and 1.3850, respectively. The isotopic H/D ratios indicate that these two bands are due to V−H stretching vibrations. In the mixed H_2O + HDO + D_2O experiment, two additional bands at 1695.3 and 1225.5 cm^{-1} were produced, suggesting that two equivalent H atoms are involved in these two modes. Accordingly, these three bands are assigned to the H_2VO molecule. The 1695.3- and 1225.5-cm^{-1} bands in the mixed H_2O + HDO + D_2O

Table 4. Calculated Vibrational Frequencies (cm^{-1}) and Intensities (km/mol) for HTaOH, H_2TaO, $TaOH_2$, and the Transition States (TS1, TS2, TS3) on the Ta + H_2O Reaction Paths

HTaOH($^4A''$)	HTaOH($^2A''$)	H_2TaO($^2A'$)	$TaOH_2$($^4A''$)	TS1	TS2	TS3
3914(183)	3894(226)	1854(109)	3789(63)	1829	1853	1989
1738(281)	1827(213)	1833(311)	3683(59)	1673	1704	1610
713(118)	748(71)	1006(144)	1595(96)	942	959	1017
556(89)	608(89)	732(30)	458(6)	649	923	998
517(151)	585(115)	594(6)	352(230)	435	817	881
308(123)	395(93)	520(73)	244(2)	1484i	1492i	1638i

Table 5. Calculated Bond Length (Å), Relative Energies (kcal/mol), and Vibrational Frequencies (cm^{-1}) of $^4\Sigma^-$ and $^2\Delta$ State VO, NbO, and TaO

	relative energy	bond length	frequency(intensity)
VO ($^4\Sigma^-$)	0	1.580	1040(256)
VO ($^2\Delta$)	+31.2	1.569	1052(270)
NbO ($^4\Sigma^-$)	0	1.711	976(170)
NbO ($^2\Delta$)	+21.6	1.699	1012(180)
TaO ($^4\Sigma^-$)	0	1.712	976(116)
TaO ($^2\Delta$)	−9.8	1.694	1028(103)

experiment are due to V−H and V−D stretching vibrations of the HDVO molecule.

The H_2VO assignment was strongly supported by DFT calculations. As shown in Figure 7, the H_2VO molecule was predicted to have a $^2A'$ ground state with nonplanar geometry and is only slightly higher in energy than the inserted HVOH molecule. The V−O, antisymmetric and symmetric VH_2 stretching vibrations were calculated at 1113, 1778, and 1815 cm^{-1}, which require scaling factors of 0.925, 0.945, and 0.942 to fit the observed values, respectively.

The 976.9-, 1665.2-, and 1704.5-cm^{-1} absorptions in the Nb + H_2O experiments were generated on broad-band photolysis and are assigned to the H_2NbO molecule following the H_2VO example. The 976.9-cm^{-1} band underwent only an 0.8 cm^{-1} deuterium isotopic shift, but was shifted to 930.4 cm^{-1} with $H_2{}^{18}O$ sample; the isotopic $^{16}O/^{18}O$ ratio 1.0500 is characteristic of a Nb−O stretching vibration. The doublet feature in the mixed H_2O + $H_2{}^{18}O$ experiment indicates the presence of only one oxygen atom. The 1665.2- and 1704.5-cm^{-1} bands showed no oxygen-18 shift with $H_2{}^{18}O$ sample, but gave deuterium counterparts at 1197.7 and 1224.0 cm^{-1} and defined H/D ratios of 1.3903 and 1.3926, respectively, indicating that these two bands are due to Nb−H stretching vibrations. As shown in Figure 5, two intermediate bands were observed at 1685.3 and 1210.9 cm^{-1}; these two bands are due to Nb−H and Nb-D stretching vibrations of the HDNbO molecule. The H_2NbO assignment was further supported by DFT calculations, which predicted a $^2A'$ ground state with Nb−O, and NbH_2 stretching vibrations at 1000, 1758, and 1785 cm^{-1}, with 179:385:142 relative intensities.

Similar bands at 986.9, 1762.3, and 1780.4 cm^{-1} in the Ta + H_2O experiments are assigned to the H_2TaO molecule. These three bands increased together on annealing. Present DFT calculations predicted that the H_2TaO molecule also has a $^2A'$ ground state with nonplanar geometry. The Ta−O, antisymmetric and symmetric TaH_2 stretching vibrations were calculated at 1006, 1833, and 1854 cm^{-1}, respectively.

There is no evidence of the metal hydride and hydroxide molecules.[39,40]

Reaction Mechanism. The reactions of transition metal cations with water molecules have been studied both experimentally and theoretically.[2−4,12] It is generally accepted that the initial interaction between transition metal cation and water molecule is to form a metal cation−water complex. Then, one hydrogen atom is transferred from oxygen to the metal, leading to the $HMOH^+$ intermediate. The reactions of transition metal atoms with water molecules are similar to the metal cation reactions. The initial step is the formation of neutral metal-water complexes, reactions 1−3.

$$V(^4F) + H_2O(^1A_1) \rightarrow VOH_2(^4B_1) \qquad \Delta E = -11.5 \text{ kcal/mol} \quad (1)$$

$$Nb(^6D) + H_2O(^1A_1) \rightarrow NbOH_2(^6A') \qquad \Delta E = -12.6 \text{ kcal/mol} \quad (2)$$

$$Ta(^4F) + H_2O(^1A_1) \rightarrow TaOH_2(^4A'') \qquad \Delta E = -8.3 \text{ kcal/mol} \quad (3)$$

From the metal−water complex MOH_2, one hydrogen atom is passed from oxygen to the metal to form the insertion product, reactions 4−6.

$$VOH_2\ (^4B_1) \rightarrow HVOH\ (^4A'') \qquad \Delta E = -43.4 \text{ kcal/mol} \quad (4)$$

$$NbOH_2\ (^6A') \rightarrow HNbOH\ (^4A'') \qquad \Delta E = -42.6 \text{ kcal/mol} \quad (5)$$

$$TaOH_2\ (^4A'') \rightarrow HTaOH\ (^4A'') \qquad \Delta E = -53.0 \text{ kcal/mol} \quad (6)$$

Although reactions 1−3 are exothermic, and all conserve spin, only the $NbOH_2$ was observed in the experiments. Our DFT calculations showed that all three HMOH (M = V, Nb, Ta) insertion molecules have quartet ground states, and reactions 4−6 are highly exothermic. The $NbOH_2$ has sextet ground state; there is spin crossing for reaction 5. Both VOH_2 and $TaOH_2$ molecules have quartet ground states- there is no spin crossing for reactions 4 and 6. These suggest that the VOH_2 and $TaOH_2$ are very short-lived, rapidly rearranging to the HVOH and HTaOH molecules. As will be discussed, the insertion molecules HMOH can further be isomerized to the H_2MO molecules. There is spin crossing from $^4A''$ HMOH to $^2A'$ H_2MO. For V and Nb, the isomerization reactions can only proceed on photolysis, while for Ta, the isomerization reaction proceeded spontaneously on annealing; this suggests that the HTaOH is also a short-lived species and it rapidly rearranges to the H_2TaO molecule.

In the V and Nb experiments, the H_2VO, H_2NbO and VO, and NbO absorptions increased markedly on broad-band photolysis at the expense of the HVOH, $NbOH_2$, and HNbOH. The H_2VO and H_2NbO molecules are most likely produced by photoinduced isomerization from the HVOH and HNbOH molecules via reactions 7 and 8, while the VO and NbO are

(39) Xiao, Z. L.; Hauge, R. H.; Margrave, J. L. *J. Phys. Chem.* **1991**, *95*, 2696.

(40) Dai, D. G.; Cheng, W.; Balasubramanian, K. *J. Chem. Phys.* **1991**, *95*, 9094.

$$HVOH(^4A'') \rightarrow H_2VO(^2A') \qquad \Delta E = +9.3 \text{ kcal/mol} \quad (7)$$

$$HNbOH(^4A'') \rightarrow H_2NbO(^2A') \qquad \Delta E = -16.3 \text{ kcal/mol} \quad (8)$$

$$HVOH(^4A'') \rightarrow VO(^4\Sigma^-) + H_2(^1\Sigma_g^+) \qquad \Delta E = +17.3 \text{ kcal/mol} \quad (9)$$

$$HNbOH(^4A'') \rightarrow NbO(^4\Sigma^-) + H_2(^1\Sigma_g^+) \qquad \Delta E = +5.0 \text{ kcal/mol} \quad (10)$$

$$HTaOH(^4A'') \rightarrow H_2TaO(^2A') \qquad \Delta E = -32.4 \text{ kcal/mol} \quad (11)$$

$$HTaOH(^4A'') \rightarrow TaO(^2\Delta) + H_2(^1\Sigma_g^+) \qquad \Delta E = -0.9 \text{ kcal/mol} \quad (12)$$

produced by H_2 elimination of the HVOH and HNbOH molecules via reactions 9 and 10. In the Ta experiments, the H_2TaO absorptions increased on annealing but the TaO absorption was not enhanced on broad-band photolysis, which indicates that reaction 11 can proceed spontaneously in the matrix, and the H_2 elimination process (reaction 12) was not observed on photolysis.

Figures 8−10 show doublet and quartet potential energy surfaces following the HMOH → MO + H_2 or H_2MO reaction paths. From doublet HMOH, the hydrogen transfers from oxygen to the metal center to form the H_2MO through transition state 1 (TS1). This process involves the breaking of the O−H bond and the formation of a M−H σ bond and a M−O Π bond. On the quartet surface, the hydrogen transfers from oxygen to hydrogen through transition state 2. This transition state leads to the H_2 elimination to form the monoxides. The H_2 elimination process involves the breaking of the H−O bond and one covalent M−H bond, with the formation of the H−H bond and a M−O π bond. The calculated structural parameters of the aforementioned transition states are shown in Figure 11.

In the V system, both the HVOH and VO molecules have quartet ground states, the reaction from HVOH to VO conserves spin, but this reaction is endothermic by ∼17.3 kcal/mol, and the transition state (TS2) lies 35.8 kcal/mol higher in energy than the $^4A''$ HVOH. There is spin crossing from $^4A''$ HVOH to $^2A'$ H_2VO, and this reaction is also predicted to be endothermic by ∼9.3 kcal/mol. Apparently, both reactions that lead to the formation of H_2VO and VO require external energy. The Nb system is quite similar to the V system, both the HNbOH and NbO molecules were predicted to have quartet ground states, the formation of NbO is endothermic by ∼5.0 kcal/mol, and there is ∼37.4 kcal/mol energy barrier from the $^4A''$ HNbOH to the $^4\Sigma^-$ NbO. From the $^4A''$ HNbOH, there is also spin crossing leading to the $^2A'$ H_2NbO molecule. Although this reaction is predicted to be exothermic by ∼16.3 kcal/mol, there is a ∼35.1 kcal/mol energy barrier. The H_2NbO absorptions greatly enhanced only on photolysis, suggesting that reaction 8 requires activation energy. In the case of Ta, the HTaOH has $^4A''$ ground state, but the ground state of TaO is a $^2\Delta$ state, the formation of both $H_2TaO(^2A')$ and TaO ($^2\Delta$) requires spin crossing. However, the formation of TaO is predicted to be exothermic by only ∼0.9 kcal/mol, while the formation of H_2TaO is exothermic by 32.4 kcal/mol, and the energy barrier leading to the TaO is much higher than the barrier leading to the H_2TaO. The formation of H_2TaO is energetically favored over the formation of TaO + H_2. The $^4A''$ and $^2A''$ states of HTaOH lie very close in energy, and spin crossing

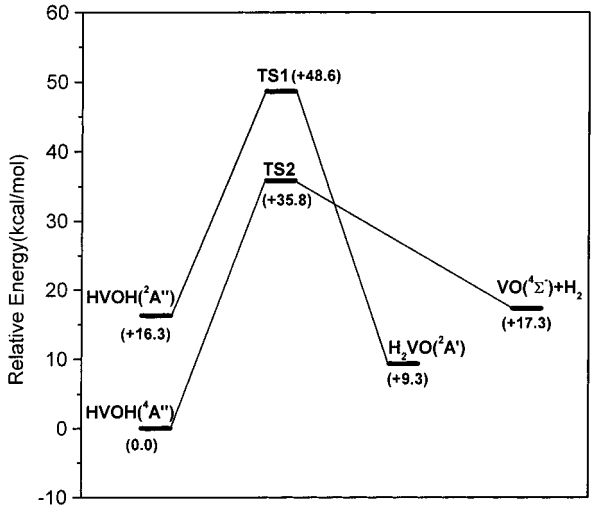

Figure 8. Potential energy surface following the reaction paths from HVOH leading to the H_2VO and VO + H_2 products. Energies given are in kcal/mol and are relative to the $^4A''$ HVOH.

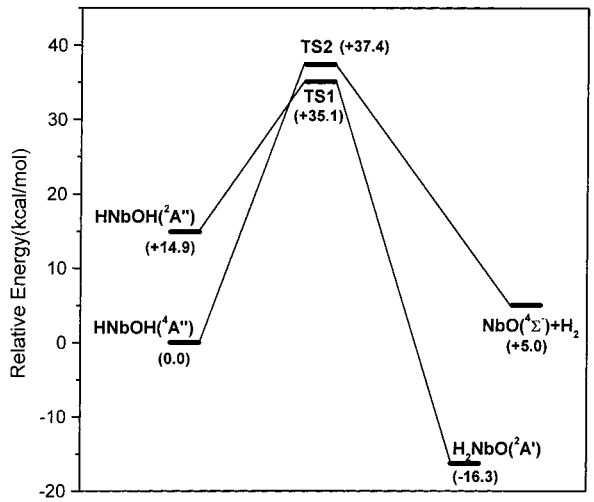

Figure 9. Potential energy surface following the reaction paths from HNbOH leading to the H_2NbO and NbO+H_2 products. Energies given are in kcal/mol and are relative to the $^4A''$ HNbOH.

has higher efficiency in matrix. Different for V and Nb, the energy barrier for the formation of H_2TaO (reaction 11) is predicted to be only 21.7 kcal/mol, lower than the reaction energy of 32.4 kcal/mol. Reaction 11 is spontaneous as evidenced by the increase of H_2TaO absorptions on annealing.

As was discussed in our previous report,[18] the only reaction path of the HScOH molecule is the H_2 elimination process to form ScO; as Sc has only three valence electrons, there are not enough electrons to satisfy chemical bonding in H_2ScO, so the H_2ScO species is unstable. For groups IV and V metal atoms, there are enough valence electrons to satisfy chemical bonding in H_2MO, so the formation of H_2MO is the major reaction path. The reactions of water with the early first-row transition metal atoms are slightly different from the early first-row transition metal cations. Both experimental and theoretical studies have shown that, for the reaction of water with metal cations, the only exothermic product is the low-lying state MO + H_2.[2,12] The H_2MO^+ (M = Sc, Ti, V) corresponds to the final intermediate on the reaction path, from this intermediate, the loss of H_2 proceeds without transition state to the final products MO^++H_2. The bonding of H_2MO^+ is also quite different from the H_2MO molecules observed in our experiments. The H_2MO^+

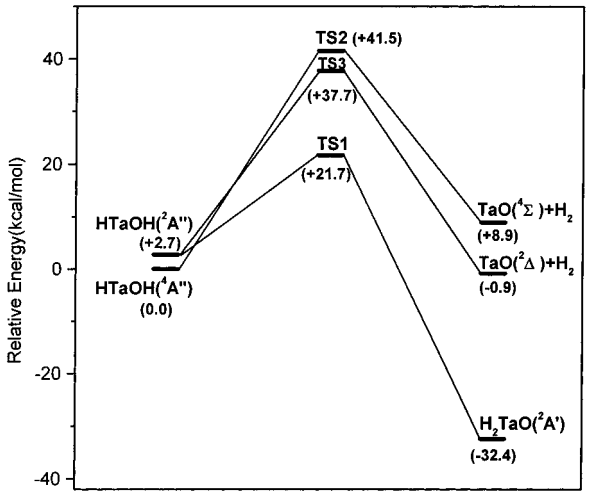

Figure 10. Potential energy surface following the reaction paths from HTaOH leading to the H_2TaO and $TaO + H_2$ products. Energies given are in kcal/mol and are relative to the $^4A''$ HTaOH.

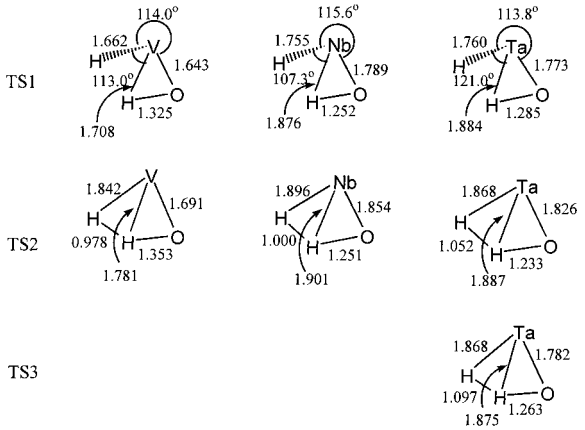

Figure 11. B3LYP calculated geometric parameters (bond length in Å, bond angle in degree) of the transition states.

species can only be viewed as ion−molecule complexes, as no M−H covalent bond exists in these H_2MO^+ complexes.

From groups IV and V metal atom and water reactions, some clear trends can be observed. For Ti, V, and Nb, the formations of both H_2MO and MO were observed. Although the reactions from HMOH to MO + H_2 (M = Ti, V, Nb) conserve spin, these reactions were predicted to be endothermic. The reactions from HMOH to H_2MO (M = Ti, V, Nb) were predicted to be slightly endothermic or exothermic, but these reactions require spin crossing. So the H_2MO and MO can only be produced on photolysis. For Zr, Hf, and Ta, the H_2MO absorptions increased on annealing, and no MO was produced on photolysis. In these three systems, the reactions from HMOH to H_2MO were predicted to be exothermic. There is no spin crossing from HHfOH to H_2HfO. For Zr and Ta, although there is spin crossing from HMOH to H_2MO, the low-spin and high-spin states HMOH are very close in energy, and the spin crossing has high efficiency.

Conclusions

The reactions of V, Nb, and Ta atoms with water molecules have been investigated using matrix isolation FTIR and density functional theoretical calculations. The V atoms reacted with water to form the inserted HVOH molecule spontaneously. The Nb atoms reacted with water to form the $NbOH_2$ complex and the inserted HNbOH molecule. Broad-band photolysis produced the H_2VO and H_2NbO molecules as well as the VO and NbO monoxides. For Ta + H_2O reactions, neither $TaOH_2$ nor HTaOH was observed, while the H_2TaO molecule was produced on annealing, and the H_2 elimination process was not observed on photolysis. The aforementioned species were identified via isotopic substitutions as well as density functional calculations. Table 6 lists the scaling factors and the observed and calculated isotopic vibrational frequency ratios of the reaction products. The results indicated that density functional theory using B3LYP and effective core potentials predicted the vibrational frequencies and normal modes of the transition metal compounds quite well.

Table 6. Scaling Factors and Observed and Calculated Isotopic Vibrational Frequency Ratios of the Observed Reaction Products

molecule	mode	scaling factor	H/D obs	H/D calcd	$^{16}O/^{18}O$ obs	$^{16}O/^{18}O$ calcd
H_2VO	sym-VH_2	0.942	1.3850	1.4026	1.0000	1.0000
	asy-VH_2	0.945	1.3827	1.3938	1.0000	1.0000
	V−O	0.925	1.0003	1.0013	1.0436	1.0442
H_2NbO	sym-NbH_2	0.955	1.3926	1.4077	1.0000	1.0000
	asy-NbH_2	0.947	1.3903	1.4025	1.0000	1.0000
	Nb−O	0.977	1.0008	1.0019	1.0500	1.0503
H_2TaO	sym-TaH_2	0.960		1.4108	1.0000	1.0000
	asy-TaH_2	0.961	1.3935	1.4073	1.0000	1.0000
	Ta−O	0.981	1.0020	1.0032	1.0536	1.0538
HVOH	V−H	0.958	1.3887	1.3995	1.0000	1.0000
HNbOH	Nb−H	0.950	1.3911	1.4060	1.0000	1.0000
$NbOH_2$	H_2O bending	0.979	1.3606	1.3641	1.0013	1.0043
VO	V−O	0.949			1.0449	1.0452
NbO	Nb−O	0.994			1.0509	1.0511
TaO	Ta−O	0.986			1.0551	1.0553

Scheme 1

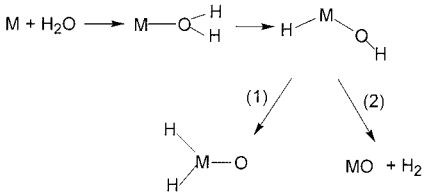

From these results together with our earlier work covering the Sc, Ti, Zr, and Hf + H_2O reactions, the following conclusions are drawn:

(1) For the reactions of early transition metal atoms with water molecules, the reaction paths shown in Scheme 1 are followed. Both reaction paths leading to the H_2MO and the MO + H_2 are exothermic. As the valence electrons of Sc cannot satisfy chemical bonding in H_2ScO, only path 2 was observed. For Ti, V, and Nb, both reaction paths were observed, while for Zr, Hf, and Ta, only path 1 was observed.

(2) The MOH_2 and HMOH species are important intermediates in the reaction paths. The stability of these intermediates depends mainly on their reactivity. For MOH_2, only the $NbOH_2$ was experimentally observed, probably due to the low efficiency of the spin crossing reaction from $NbOH_2$ to HNbOH. The other MOH_2 are short-lived species, rapidly rearranging to the HMOH molecules. For HMOH, the HTiOH, HZrOH, HVOH, and HNbOH were observed, while the HHfOH and HTaOH molecules are short-lived species and were not observed in experiments.

Acknowledgment. This work is supported by NSFC (Grant 20003003) and the Chinese NKBRSF.

JA003072Z